Angewandte Chemie
Eine Zeitschrift der Gesellschaft Deutscher Chemiker

Supporting Information

A Potassium Diboryllithate: Synthesis, Bonding Properties, and the Deprotonation of Benzene

Takuto Ohsato, Yuri Okuno, Shintaro Ishida, Takeaki Iwamoto, Ka-Ho Lee, Zhenyang Lin, Makoto Yamashita,* and Kyoko Nozaki**

anie_201605005_sm_miscellaneous_information.pdf

Supporting Information for

General

All manipulations involving the air- and moisture-sensitive compounds were carried out in glovebox (KIYON, Korea and ALS Technology, Japan) under argon atmosphere. *n*-Hexane was purified by passing through a solvent purification system (Grass Contour). Benzene, cyclohexane, purified *n*-hexane, 2,2,4,4-tetramethylpentane were degassed and were dried by stirring with Na/K alloy at room temperature in the glovebox prior to use. Benzene-d_6 was dried over Na/Ph_2C=O and was distilled under reduced pressure. Cyclohexane-d_{12} was dried by filtering through a pad of activated alumina and subsequent stirring with Na/K alloy at room temperature in the glovebox prior to use. Lithium dispersion (purchased from Kanto Chemical Co., Inc., containing 1% sodium) was washed with *n*-hexane before the use to make a lithium powder. Na/K alloy (1/4 molar ratio) was prepared by contacting two metals (Na: Kanto Chemical, K: Strem Chemical), which were freshly pealed to remove the inactive outside layer, in glovebox (endothermic reaction). Adamantane was used as received. NMR spectra were recorded at 22 °C on 500, 400, or 300 MHz spectrometers unless otherwise noted. Solid-state ^{7}Li NMR spectra were recorded on JEOL JNM-ECA800 MHz spectrometer in Tohoku University with setting of ^{7}Li: 310.96 MHz; single pulse/MAS; 2.5 mm sample tube; 10000 Hz. Chemical shifts are reported in ppm relative to the residual protiated solvent for ^{1}H, external LiCl in D_2O for ^{7}Li, deuterated solvent for ^{13}C, and external $BF_3{\cdot}OEt_2$ for ^{11}B nuclei. Data are presented in the following space: chemical shift, multiplicity (s = singlet, d = doublet, t = triplet, sept = septet, m = multiplet, br = broad, brs = broad singlet), coupling constant in hertz (Hz), and signal area integration in natural numbers. Bromoborane **1** and hydroborane **3** were synthesized according to the literature.[1] Elemental analyses were performed at the A Rabbit Science Co., Ltd. Melting points (m.p.) were determined with a MPA100 OptiMelt (Tokyo Instruments, Inc.) and were uncorrected. X-ray crystallographic analysis was performed on VariMax/Saturn CCD diffractometer.

Preparation of 2 in cyclohexane

In a glovebox, a suspension of lithium powder (208 mg 30.0 mmol, containing 1% sodium) in cyclohexane (3.50 mL) was stirred with glass-coated stirring bar for 4 h at room temperature to give Li grains exhibiting metallic luster. To the resulting suspension, **1** (1.17 mg, 2.50 mmol), Na/K (1/4 in molar ratio, 179 mg, 4.99 mmol) and cyclohexane (9.00 mL) were added at the room temperature. The resulting suspension was further stirred at room temperature for 47 h to afford a gray suspension. The resulting suspension was filtered through pad of Celite to remove an excess amount of reductant and the volatiles were removed from the filtrate under reduced pressure. Recrystallization of the residue from cyclohexane/*n*-hexane yielded a

pale yellow microcrystal of **2** (651 mg, 63%). Crystals suitable for X-ray analysis were separately prepared (see below). ^{1}H NMR (C_6D_{12}, 500.2 MHz) δ 0.87 (d, J = 7 Hz, 24H), 1.04 (d, J = 7 Hz, 24H), 3.13 (sep, J = 7 Hz, 8H), 6.14 (s, 4H), 6.98 (d, J = 8 Hz, 8H), 7.07 (dd, J = 7 Hz, 7 Hz, 4H); ^{7}Li{^{1}H} NMR (C_6D_{12}, 194.4 MHz) δ 4.7 [brs, fwhm (full width at half maxima) = 67 Hz]; ^{7}Li{^{1}H} NMR (CPMAS, 310.96 MHz) δ 5.5 [brs, fwhm = 243 Hz]; ^{11}B{^{1}H} NMR (C_6D_{12}, 160.5 MHz) δ 43 (brs); ^{13}C{^{1}H} NMR (125.8 MHz) δ 24.4 (CH_3), 24.9 (CH_3), 28.6 (CH), 118.9 (CH), 123.3 (CH), 126.1 (CH), 146.4 (4°), 147.9 (4°); mp: 92.4-100.5 °C; Anal. Calcd. for $C_{52}H_{72}B_2KLiN_4$: C, 76.09; H, 8.84; N, 6.83. Found: C, 76.09 (coincidentally matched to the calculated value); H, 9.17; N, 6.80.

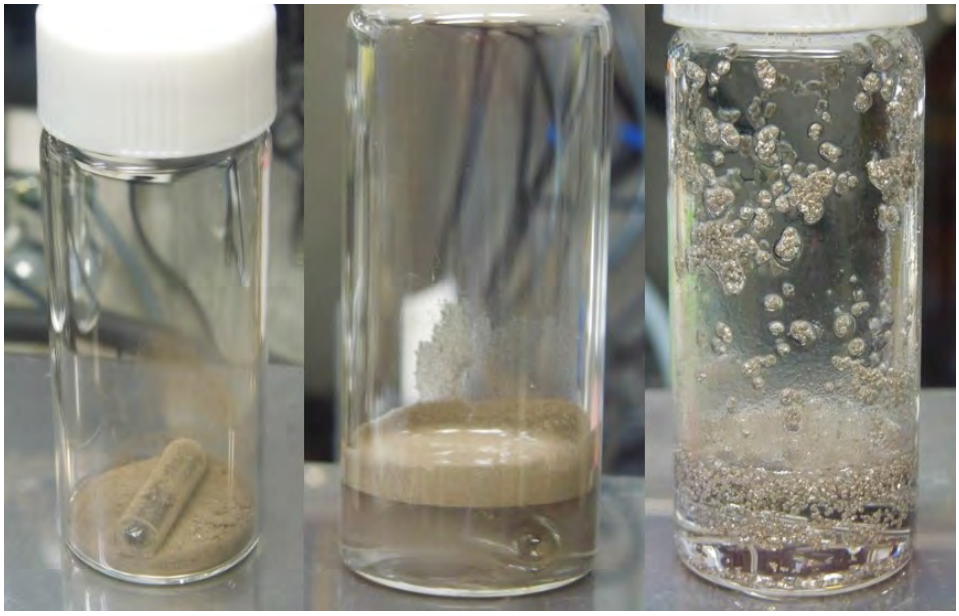

Figure S1. Pictures for setup the reaction: (left) glass-coated stirring bar and lithium powder in a 30 mL vial; (center) after addition of solvent; (right) the resulting Li grains after stirring Li powder at RT.

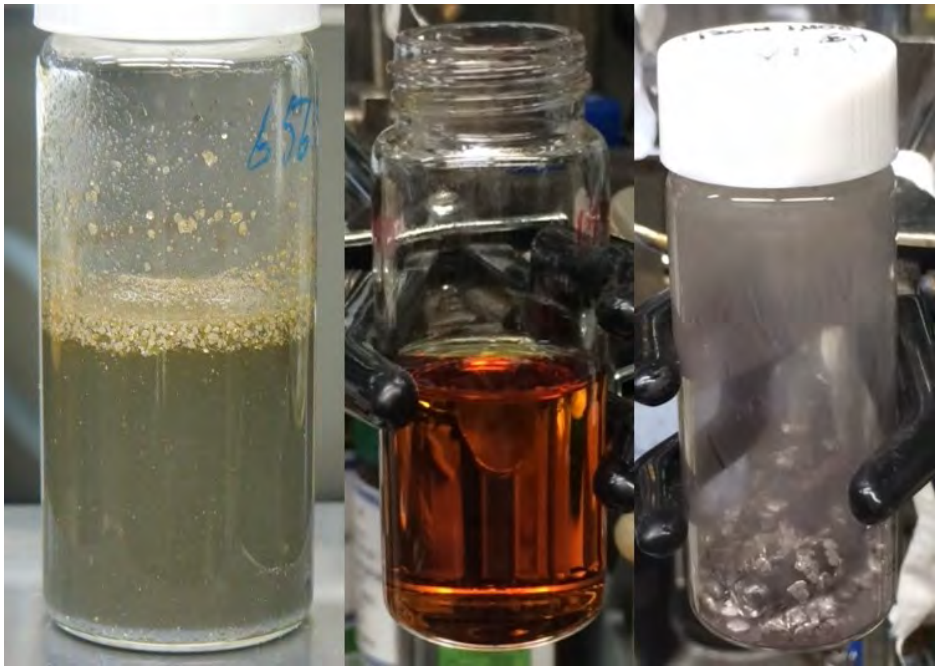

Figure S2. Pictures after the reaction: (left) just prepared reaction mixture; (center) crude solution by filtration through a pad of Celite; (right) residue of the excess reductant and salts.

Figure S3. Pictures during recrystallization: (left) crude solution left at –30 °C for overnight; (right) yellowish solids of **2** after quick pipetting out of solvent with precooled Pasteur pipette and washing twice with cold hexane. (If a saturated solution was used for recrystallization, it is very difficult to remove mother liquor. We recommend to use unsaturated solution for obtaining **2** with high purity.)

Preparation of single crystals of 2 suitable for X-ray crystallographic analysis

In a glovebox, a suspension of lithium powder (41.6 mg, 6.00 mmol) in 2,2,4,4-tetramethylpentane (0.100 mL) was stirred with glass-coated stirring bar for 2 h at room temperature. To the resulting suspension, **1** (234 mg, 0.500 mmol), Na/K (1/4) (53.8 mg, 1.50 mmol), and 2,2,4,4-tetramethylpentane (2.50 mL) were added at room temperature. The resulting suspension was further stirred for 24 h at room temperature to afford a gray suspension. The resulting suspension was filtered to remove an excess amount of reductant and the filtrate was cooled down to –30 °C to give pale yellow single crystals of **2** suitable for X-ray crystallographic analysis.

Solid state ^{7}Li NMR study for 2

Solution ^{7}Li NMR spectrum of **2** was illustrated in Figure S4(a). Solids of **2** was placed into a 2.5 mm sample tube, then ^{7}Li NMR spectrum was recorded with 10000 Hz rotation [Figure S4(b)]. A broad signal at 2.2 ppm may be a signal of trace LiOH in **2**. Then, the sample tube was opened and **2** was exposed to the air for 5 min. Then the sample tube was closed and ^{7}Li NMR spectrum was measured again [Figure S4(c)]. In Figure S4(c), a broad signal appeared at 1.0 ppm may be assignable to LiOH derived from hydrolysis of **2**. The slightly different chemical shift of this signal from that of the authentic LiOH [Figure S4(d)] may be caused by a slightly different environment of LiOH surrounded by organic molecules.

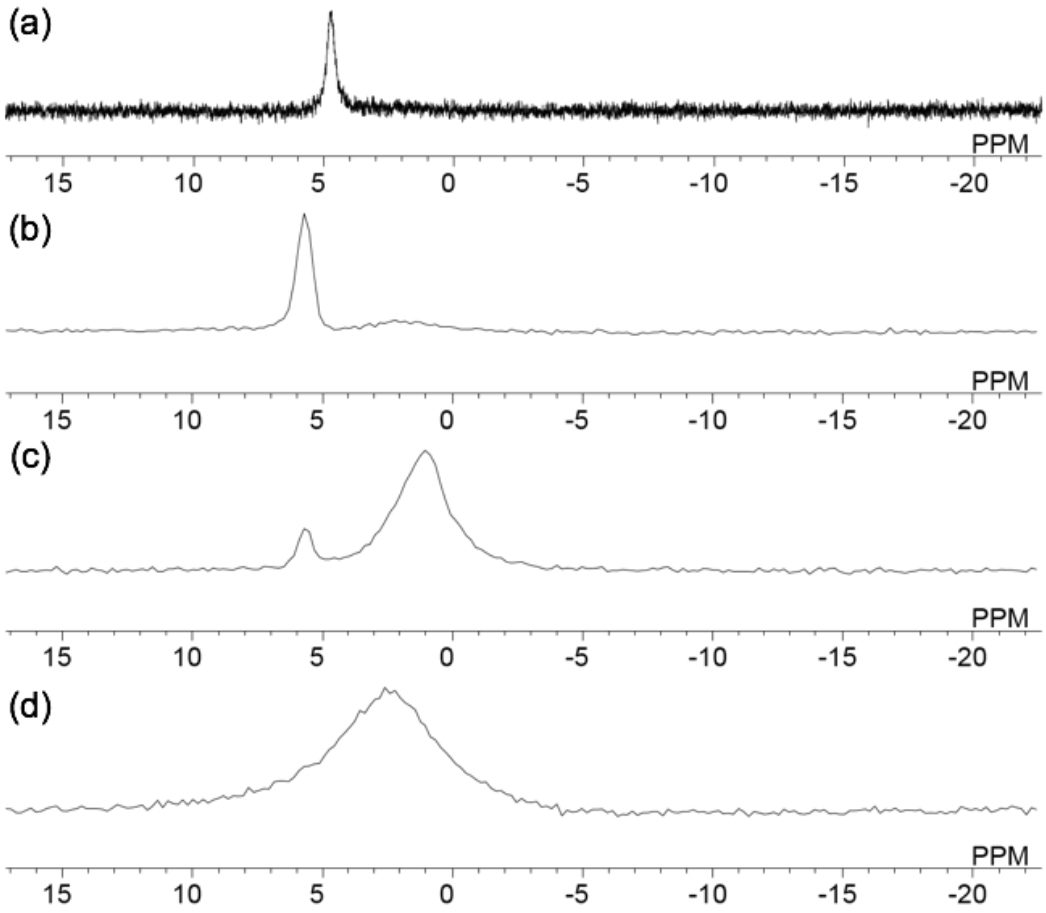

Figure S4. $^{7}Li\{^{1}H\}$ NMR spectra referenced with solid LiCl as 0 ppm (all the spectra were processed with 1.0 Hz of broadening factor): (a) **2**: C_6D_{12} solution, (b) **2**: solid state, (c) **2** after exposure to the air for 5 min: solid state, (d) LiOH (authentic sample): solid state

NMR yield for the formation of 2 in C_6D_{12}

In a glovebox, lithium powder (16.6 mg 2.40 mmol) was added to cyclohexane-d_{12} (0.100 mL). The resulting suspension was stirred for 1 h with glass-coated stirring bar at room temperature to give silver grains. To the resulting suspension, **1** (93.4 mg, 0.200 mmol), Na/K (1/4) (21.4 mg, 0.596 mmol), LiBr (52.1 mg, 0.600 mmol), and cyclohexane-d_{12} (0.900 mL) was added. The resulting suspension was further stirred at room temperature for 24 h to afford a gray suspension. To the resulting suspension, 93.9 M adamantane/cyclohexane-d_{12} solution (200 μL, 18.8 μmol) was added. The resulting mixture was filtered to remove an excess amount of reductant. An aliquot of the resulting filtrate was taken into a screw-capped NMR tube. The resulting sample was analyzed by ^{1}H NMR spectrum to determine the NMR yield of **2** (92.1 μmol, 92%, Figure S5). Because of overlapping two septet signals of **2** and byproduct **3** around 3.1 ppm, half of the integral ratio for each signal was compared with the sum of signals (16H) for adamantane around 1.8 ppm.

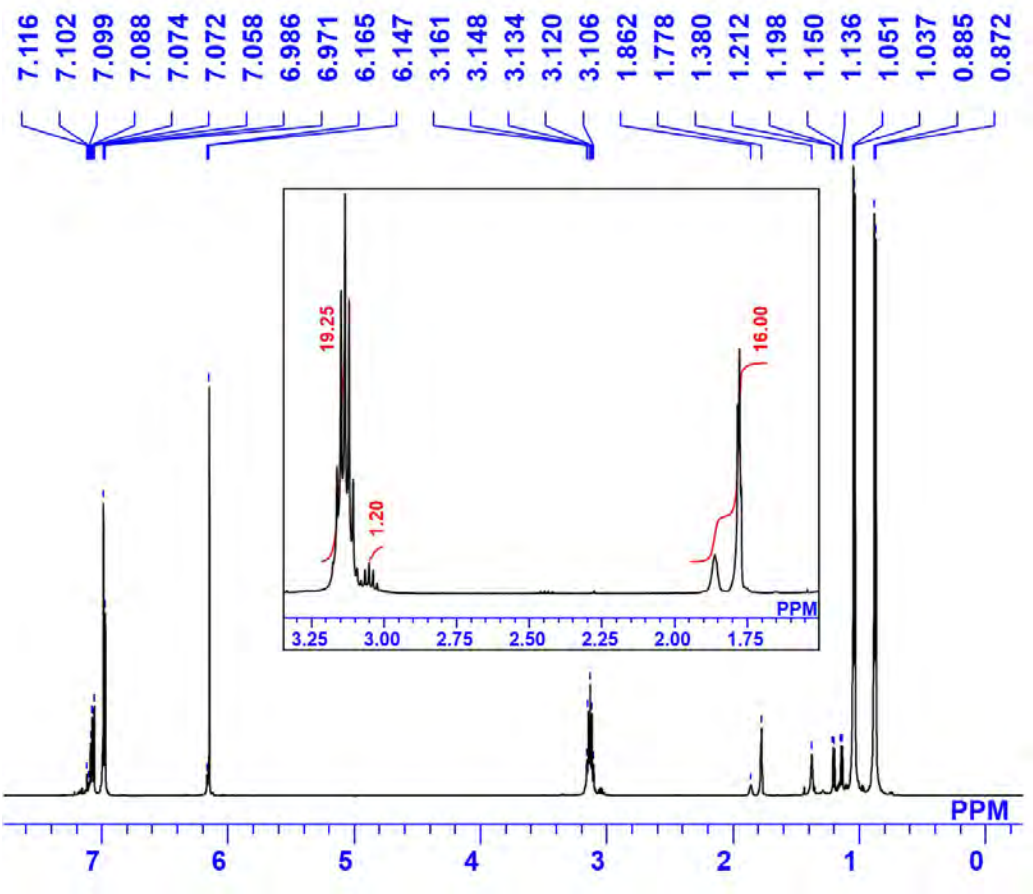

Figure S5. ^{1}H NMR spectrum to estimate the NMR yield for the formation of **2**

Reaction of 2 with benzene

In a glovebox, isolated crystals of **2** (20.0 mg, 24.4 μmol) was dissolved in benzene (200 μL) at room temperature. The resulting solution was stirred at room temperature for 10 h and the volatiles were removed under reduced pressure. To the reaction mixture, an adamantane/C_6D_6 solution (89.2 mM, 620 μL, 55 μmol) was added, followed by filtration to remove the insoluble salt. An aliquot of the resulting filtrate was taken into a screw-capped NMR tube. The resulting sample was analyzed by ^{1}H NMR spectrum to determine the NMR yield (Figure S3, **4**: 41.5 μmol, 85%, **3**: 7.3 μmol, 15%) by comparison with spectroscopic data of previously reported **4** and **3**.[1-2] The ^{1}H NMR spectrum for estimation of the yields is illustrated in Figure S6.

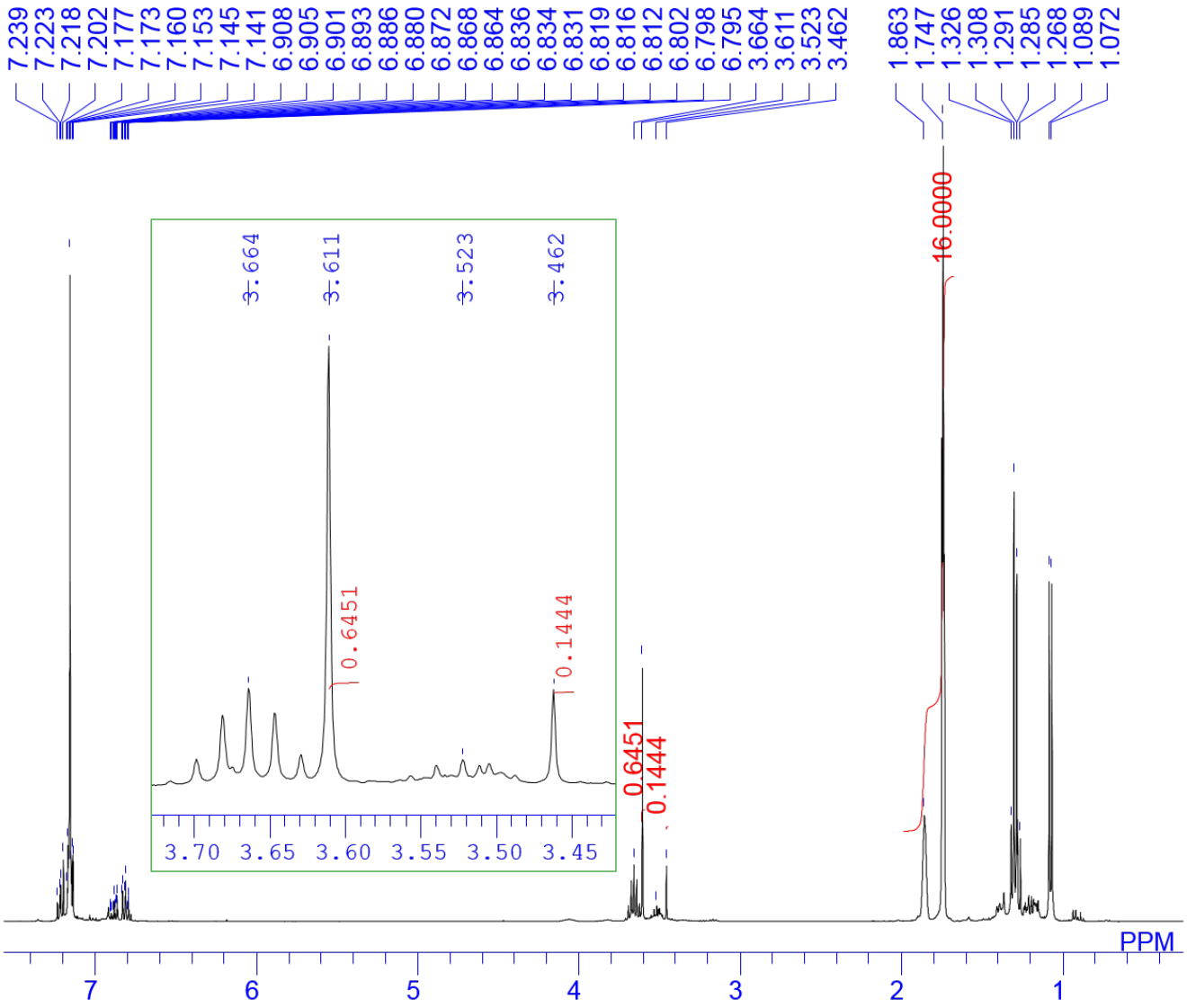

Figure S6. ^{1}H NMR spectrum to estimate the NMR yield for the reaction of **2** with benzene

Kinetic analysis for the reaction of 2a with benzene and benzene-d_6

In a glovebox, isolated crystals of **2** (10.2 mg, 12.4 μmol for C_6H_6, 11.2 mg, 13.6 μmol for C_6D_6) was dissolved in 106 μM adamantane/C_6D_{12} (383 μL, 5.50 μmol) at room temperature and the subsequent addition of benzene (218 μL, 2.44 mmol) or benzene-d_6 (216 μL, 2.44 mmol). Decay of **2** was monitored with the integral ratio of alkene protons over that of adamantane by ^{1}H NMR spectrum at 20 °C. The observed rate constants k_{obs} were determined by pseudo-first order plot resulting from concentration of unsaturated diboryllthate depending on time as summarized in Figure S7.

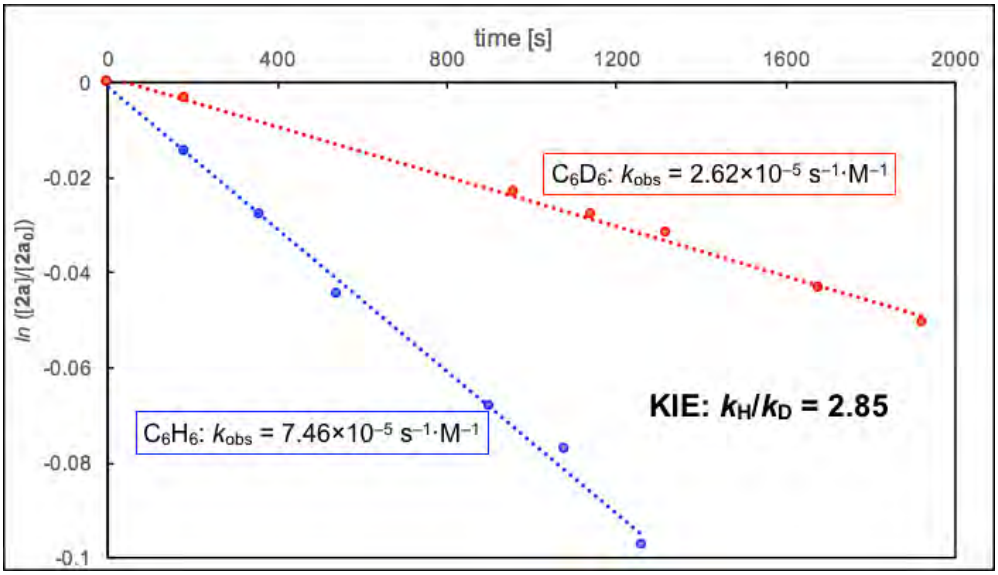

Figure S7. First-order plot for consumption of **2** reacting with benzene and benzene-d_8 at 20 °C

Details for X-ray crystallography

In each case a suitable crystal was mounted with a fluorinated mineral oil to the glass fiber and transferred to the goniometer of a VariMax Saturn CCD diffractometer with graphite-monochromated Mo Kα radiation (λ = 0.71070 Å). All the following procedure for analysis, Yadokari-XG 2009 was used as a graphical interface.[3] The structures were solved by direct methods with (SIR-2014)[4] and refined by full-matrix least-squares techniques against F^2 (SHELXL-2014).[5] The intensities were corrected for Lorentz and polarization effects or NUMABS program (Rigaku 2005). The non-hydrogen atoms were refined anisotropically. Hydrogen atoms were placed using AFIX instructions. The resulting CIF file was deposited to Cambridge Crytallographic Data Center. All the details about crystallographic data for **2·C_9H_{20}** are summarized in Table S1.

Table S1. Crystallographic data and structure refinement details for **2·C_9H_{20}**

	2·C_9H_{20}
CCDC deposit #	865529
formula	$C_{52}H_{72}B_2KLiN_4 \cdot C_9H_{20}$
fw	1077.29
T (K)	93(2)
λ (Å)	0.71075
cryst syst	Monoclinic
space group	C_2/c
a, (Å)	32.60(4)
b, (Å)	12.845(10)
c, (Å)	22.01(2)
α , (deg)	90
β , (deg)	131.977(3)
γ , (deg)	90
V, (Å^3)	6852(12)
Z	4
Dcalc, (g / cm^3)	1.044
μ (mm^{-1})	0.118
F(000)	2368
cryst size (mm)	0.18×0.15×0.15
2θ range, (deg)	3.172-24.998
reflns collected	22897
indep reflns/Rint	5946/0.0682
params	409
GOF on F^2	0.999
R_1, wR_2 [I>2σ(I)]	0.0612, 0.1448
R_1, wR_2 (all data)	0.0925, 0.1758

Details for computation

For structural optimization of 2 at the ground state, NMR chemical shift (GIAO) calculation, AIM analysis, and NBO analysis

From the obtained crystal structure of **2**, the molecular geometry of **2a** was optimized at B3LYP[6]/6-31+G(d)[7] level by using Gaussian 09 (rev. D.01) package.[8] The optimized structure was confirmed to have no imaginary frequency and could reproduce the X-ray structure (Figure S8 for labels of atoms, XMol file for visualization is also available as Supporting Information). The HOMO orbital of the optimized structure was illustrated in the main text. At the optimized structure, natural bond orbital (NBO) analysis was performed at the same level of calculation by using NBO 3.0 package embedded in Gaussian program.[9] The ^{7}Li NMR chemical shift calculation was achieved by using the Gauge-Independent Atomic Orbital (GIAO) method[10] at B3LYP/6-311++G(2d,p) level. The obtained GIAO nuclear magnetic shielding tensor was corrected with that of the independently calculated $Li(H_2O)_4^+$. From the formatted checkpoint file of the structural optimization, atoms-in-molecule (AIM) analysis was also performed by using AIMALL program[11] to form molecular graph of **2** (Figure S9) as illustrated in the main text. The obtained NPA charges and parameters on the bond critical points (BCPs) are summarized in Tables S2 and S3.

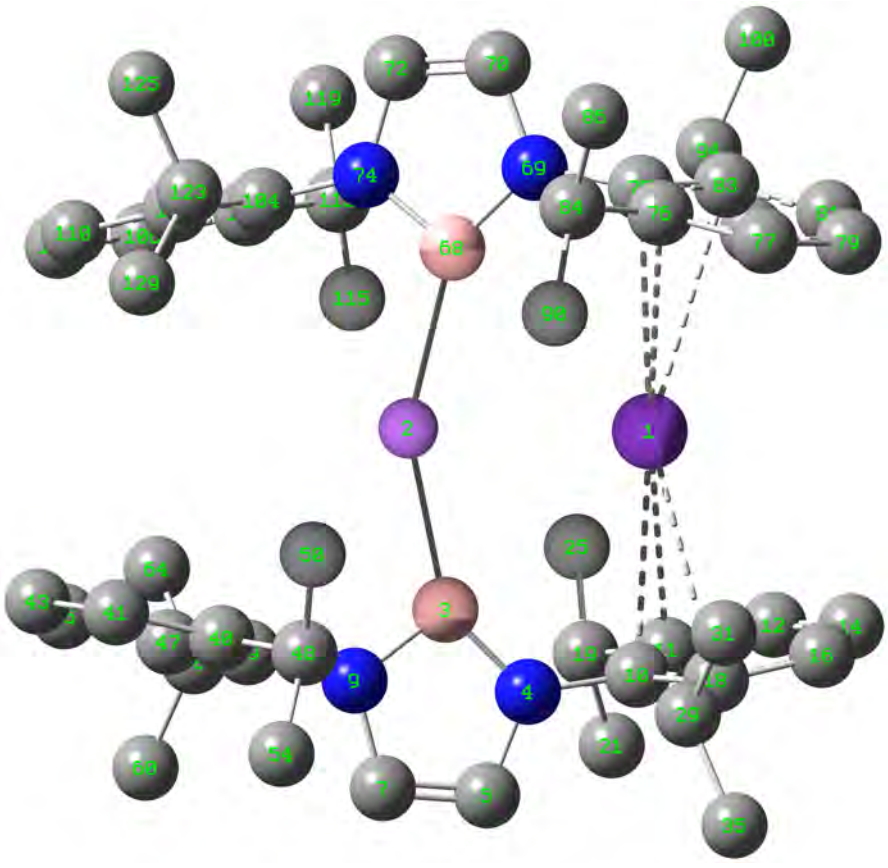

Figure S8. Optimized structure of **2** with labels of atoms (hydrogen atoms are omitted for clarity, labeling can also be found in XMol file)

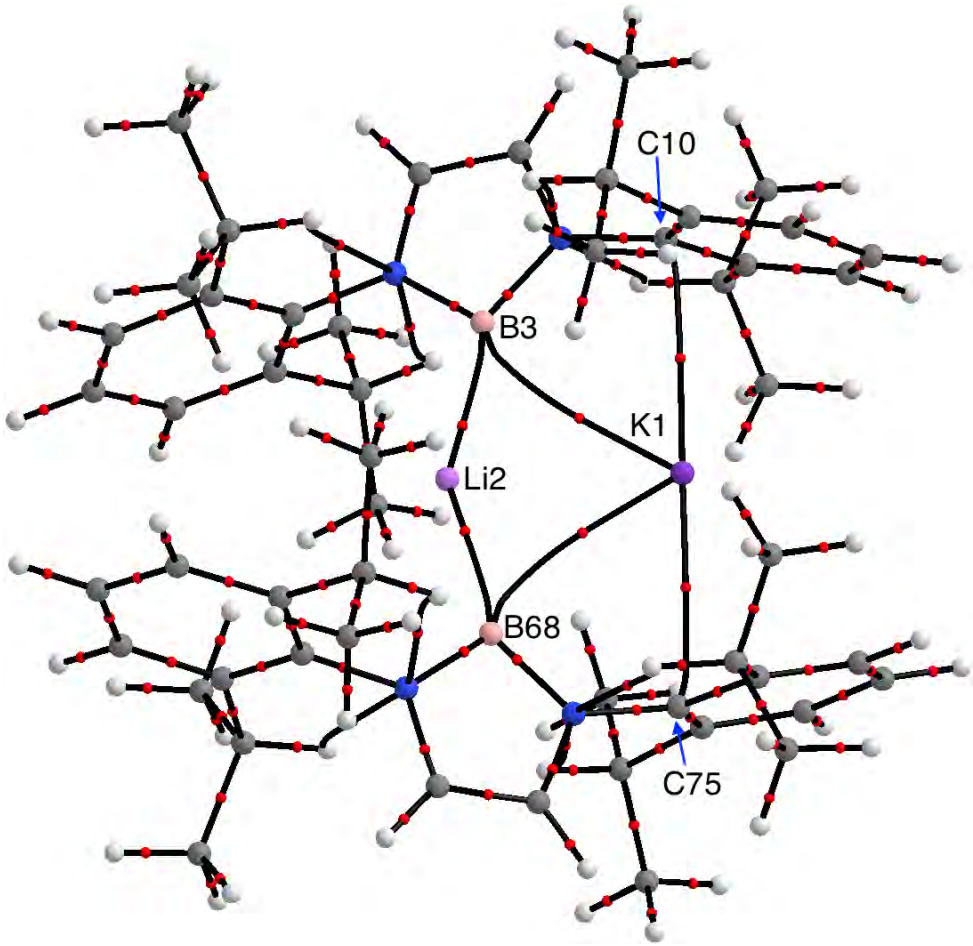

Figure S9. Molecular graph of **2** produced by AIM analysis [gray: carbon, white: hydrogen, blue: nitrogen, pale orange: boron, light purple: lithium, purple: potassium; red spheres: bond critical points, solid lines: bond paths; , numberings are based on the result illustrated in Figure S8]

Table S2. Summary of natural population analysis for **2** (labels corresponds to those in Figure S8)

atom	label	natural charge	atom	label	natural charge	atom	label	natural charge	atom	label	natural charge
K	1	0.65877	H	34	0.22474	H	67	0.22615	C	100	-0.66606
Li	2	0.51631	C	35	-0.66636	B	68	0.1228	H	101	0.2424
B	3	0.12306	H	36	0.24244	N	69	-0.7205	H	102	0.23942
N	4	-0.72056	H	37	0.23954	C	70	-0.11751	H	103	0.22815
C	5	-0.11799	H	38	0.22788	H	71	0.23558	C	104	0.17882
H	6	0.23573	C	39	0.17889	C	72	-0.09337	C	105	-0.02023
C	7	-0.09317	C	40	-0.02033	H	73	0.23887	C	106	-0.23841
H	8	0.23884	C	41	-0.23843	N	74	-0.71141	H	107	0.23508
N	9	-0.71121	H	42	0.23507	C	75	0.17928	C	108	-0.23475
C	10	0.17944	C	43	-0.23487	C	76	-0.02324	H	109	0.23896
C	11	-0.02405	H	44	0.23892	C	77	-0.24319	C	110	-0.23308
C	12	-0.24396	C	45	-0.23313	H	78	0.24474	H	111	0.23638
H	13	0.24494	H	46	0.23623	C	79	-0.24356	C	112	-0.01944
C	14	-0.24391	C	47	-0.01928	H	80	0.24746	C	113	-0.29968
H	15	0.24762	C	48	-0.29949	C	81	-0.24746	H	114	0.26562
C	16	-0.24704	H	49	0.26587	H	82	0.24385	C	115	-0.66165
H	17	0.24389	C	50	-0.66182	C	83	-0.0369	H	116	0.23962
C	18	-0.03595	H	51	0.23951	C	84	-0.3025	H	117	0.23209
C	19	-0.30276	H	52	0.23236	H	85	0.27738	H	118	0.22625
H	20	0.27768	H	53	0.22607	C	86	-0.66773	C	119	-0.66694
C	11	-0.02405	C	54	-0.66694	H	87	0.22633	H	120	0.22801
C	12	-0.24396	H	55	0.22803	H	88	0.2396	H	121	0.23175
H	13	0.24494	H	56	0.23174	H	89	0.24261	H	122	0.24031
C	14	-0.24391	H	57	0.24033	C	90	-0.65665	C	123	-0.2986
H	15	0.24762	C	58	-0.29871	H	91	0.23684	H	124	0.26488
C	16	-0.24704	H	59	0.26472	H	92	0.24371	C	125	-0.66621
H	17	0.24389	C	60	-0.66622	H	93	0.22374	H	126	0.22814
C	18	-0.03595	H	61	0.22806	C	94	-0.30575	H	127	0.23875
C	19	-0.30276	H	62	0.2387	H	95	0.27726	H	128	0.23278
H	20	0.27768	H	63	0.23279	C	96	-0.65539	C	129	-0.66232
C	31	-0.65564	C	64	-0.66209	H	97	0.2262	H	130	0.23322
H	32	0.22581	H	65	0.23301	H	98	0.24523	H	131	0.24331
H	33	0.2449	H	66	0.24332	H	99	0.22327			

Table S3. Summary of parameters obtained by AIM analysis for **2** [electron density $\rho(r)$, Lapacian of $\rho(r)$, bond ellipticity ε at bond critical points related to B, Li, K, and C(ipso to N) atoms]

atoms for BCP	$\rho(r)$ (e/a_0^3)	$\nabla^2\rho(r)$ (e/a_0^5)	ε
K1–B3	0.009453	0.021209	0.110517
Li2–B3	0.026049	0.068228	0.017073
K1–C10	0.00954	0.035475	0.824388
K1–B68	0.009664	0.021771	0.10649
Li2–B68	0.025859	0.067572	0.017814
K1–C75	0.00944	0.035044	0.865435

For elucidation of detailed reaction pathway for deprotonation of benzene by 2

The full models for the species involved in the reactions were employed in the calculations. The molecular geometry optimizations were performed without constraints at the Becke3LYP (B3LYP) level of density functional theory.[6] The 6-31G(d) basis set was used for all the atoms, except for Li and K atoms (the 6-31+G(d) basis set was used) and H atom that involved in the C–H bond cleavage (the 6-31G(d,p) basis set was used).[7] Frequency calculations at the same level of theory were performed. The nature of the calculated stationary points were verify as minima (zero imaginary frequency) and transition states (one imaginary frequency). For the NBO analysis of $\mathbf{TS_{2\text{-}6}}$, single point calculation was performed with the same level of theory.

To reduce the overestimation of the entropy contribution in the gas-phase results, corrections of −2.6 kcal/mol (or +2.6 kcal/mol) in free energies were made for 2-to-1 (or 1-to-2) transformations.[12] To take dispersion and solvation effects into account, we carried out single-point energy calculations at the B3LYP-D3/6-311+G(d,p) level with the optimized structures,[6-7,13] employing a continuum medium using UAKS radii on the conductor-like polarizable continuum model (CPCM).[14] Following the reaction conditions, benzene was employed as the solvent in these single-point energy calculations. Unless specifically noted, the entropy- and solvation-corrected free energies were used in all of the discussions. All the calculations were performed with Gaussian 09 (rev. D.01) package.[8]

All the obtained structures are attached as Supporting Information in .xyz format.

Pathways not described in the main text

Less probable TSs for deprotonation of benzene by 2 and subsequent formation of phenylborane 6

One can expect **2** deprotonates benzene through a π-coordination of benzene to Li^+ to give **7** as other possible pathway for deprotonation of benzene (Scheme S1). However, the $\mathbf{TS_{2\text{-}7}}$ has activation energy of 31.6 kcal/mol, which is 3.0 kcal/mol higher than that of $\mathbf{TS_{2\text{-}6}}$. As another possible pathway, we also found nucleophilic attack of boryl anion to benzene coordinating to K^+ to give potassium (boryl)[(boryl)cyclopentadienyl]lithate intermediate **18**, which may liberate (boryl)(hydrido)lithate **10** and phenylborane **4** via hydride migration to Li^+. However, the activation energy of this process further higher than that of deprotonation with coordination of Dip ring to K^+.

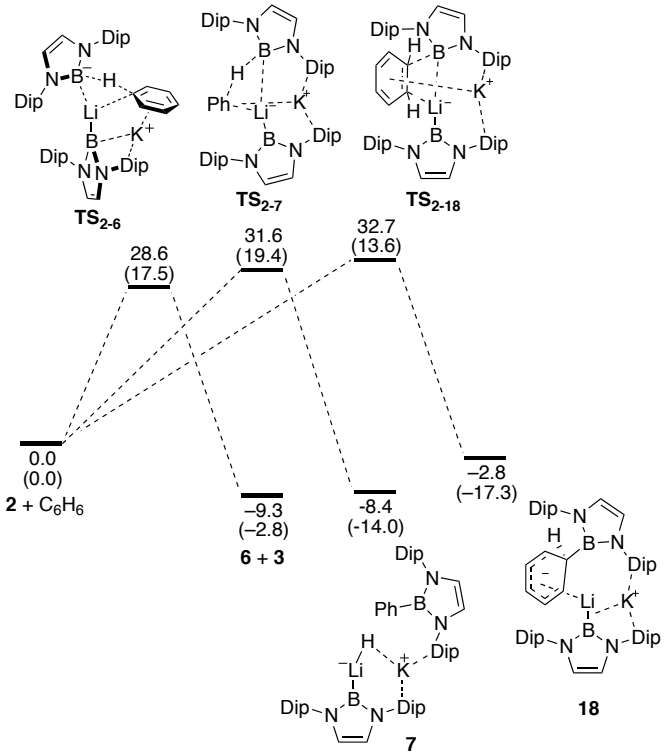

Scheme S1. Energy profiles calculated for the possible activation of benzene by **2**. The relative Gibbs free energies and electronic energies (in parentheses) are given in kcal/mol.

Two TSs for complexation of 6 with 3

The complexation of **6** with **3** to give **7** was calculated to have two small TSs (Scheme S2). Hydride on the boron atom in **3** directly access to the positively charged K^+ with an activation energy of 9,8 kcal/mol to afford **19**. Then, rotation of hydroborane moiety in **19** induced coordination of Dip ring to K^+ and dissociation of B–H moiety from K^+ to result in the formation of **7** through $\mathbf{TS_{19\text{-}7}}$ with activation energy of 2.5 kcal/mol.

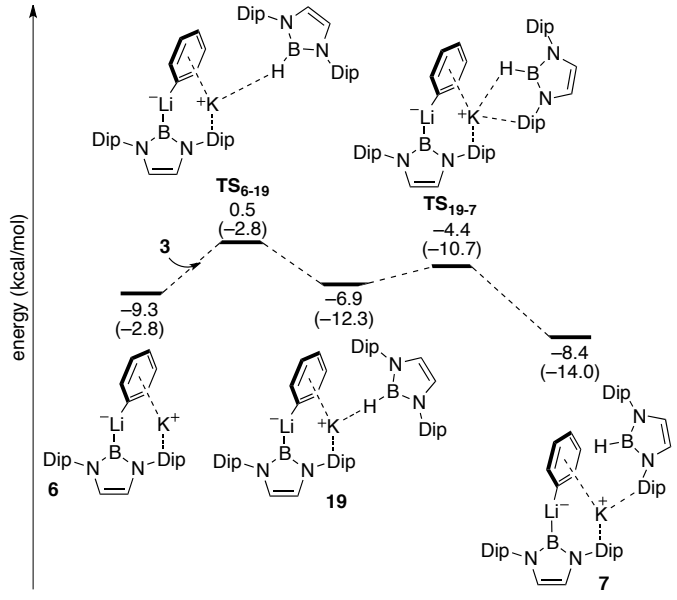

Scheme S2. Energy profiles calculated for complexation of **6** with **3**. The relative Gibbs free energies and electronic energies (in parentheses) are given in kcal/mol.

Possibility for deprotonation of benzene with 6 followed by hydride/phenyl exchange to form phenyborane 4

From (boryl)(phenyl)lithate intermediate **6**, several possible pathways were found to produce phenylborane **4** (Scheme S3). The most straightforward pathway is initiated by a coordination of benzene to **6** to afford **20** through red-colored route. The resulting **20** undergoes deprotonation of coordinating benzene molecule by boryl anion moiety to give **21** through $\mathbf{TS_{20\text{-}21}}$ (24.6 kcal/mol from **6**). Although coordination of Dip group to potassium in **21** is weak as confirmed by that the dissociation of potassium diphenyllithate **22** requires only small difference in energy (1.8 kcal/mol), the phenyl group in diphenyllithate moiety can attack to the boron atom in **21** through $\mathbf{TS_{21\text{-}23}}$. The intermediate **23** is further rearranged with small activation energy of 7.2 kcal/mol at $\mathbf{TS_{23\text{-}24}}$ to result in the formation of **24**, which further liberates phenylborane **4** and potassium (hydrido)(phenyl)lithate **13**. As alternative route, a pathway involving the second equivalent of benzene molecule was also found (blue-colored). Sequential double solvation of **6** with two benzene molecules affords the intermediates **25** and **26**, in which the latter undergoes deprotonation of benzene by boryl anion moiety through $\mathbf{TS_{26\text{-}27}}$ (22.4 kcal/mol from **6**). Loss of one benzene molecule from **27** and subsequent rearrangement of **28** through dissociation of potassium diphenyllithate **22** generates **21**, which is the identical intermediate the red-colored route. The intermediate **28** is also accessible through deprotonation of benzene in **25** possessing one benzene molecule through $\mathbf{TS_{25\text{-}28}}$ with an activation energy of 23.5 kcal/mol from **24**. All the activation energy at the highest TSs in these possible pathways are higher than that (18.1 kcal/mol) of the most feasible pathway which is described in the main text.

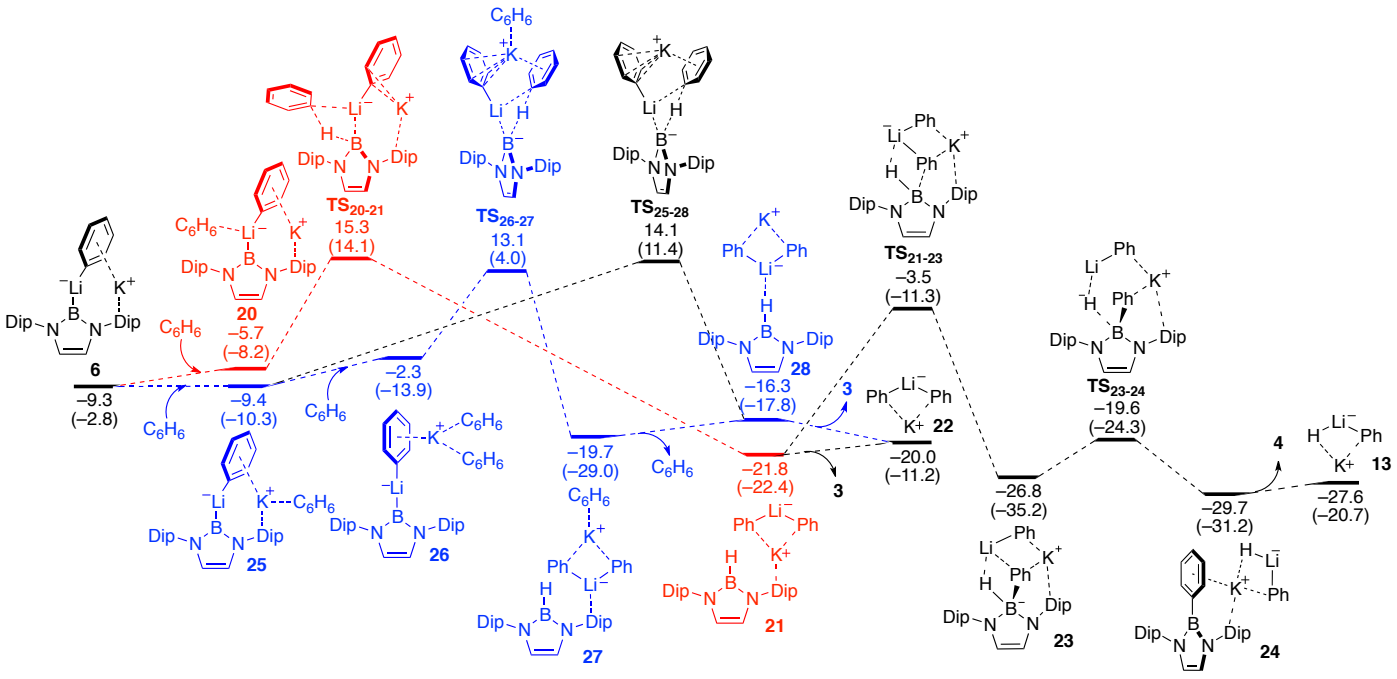

Scheme S3. Energy profiles calculated for deprotonation of benzene by **6**. The relative Gibbs free energies and electronic energies (in parentheses) are given in kcal/mol.

Less probable TSs for deprotonation of the second benzene by 10

The red-colored pathway (**10**, **11**, $\mathbf{TS_{11\text{-}12}}$, **12**, **13**, **14**, $\mathbf{TS_{14\text{-}15}}$, **15**) in Scheme S4 is the most probable pathway, which is described in the main text. From the intermediate **11**, another possible (blue-colored)

pathway was also found. Similar to the blue-pathway in Scheme S3, second equivalent of benzene coordinates to K^+ in **11** to form the intermediate **29**. The subsequent deprotonation of benzene by boryl anion moiety through $\mathbf{TS_{29\text{-}30}}$ afforded the intermediate **30** with a slightly (1.2 kcal) higher activation energy than that of $\mathbf{TS_{11\text{-}12}}$. Liberation of benzene from **30** afforded the intermediate **12** which is linked to the red-colored pathway. Also, coordination of benzene to Li^+ in **10** resulted in the formation of an intermediate **31**, which underwent deprotonation of coordinating benzene to be connected to the intermediate **14** via $\mathbf{TS_{31\text{-}14}}$. This route has much higher activation energy at $\mathbf{TS_{31\text{-}14}}$. Thus, the pathway described in the main text is the most probable pathway.

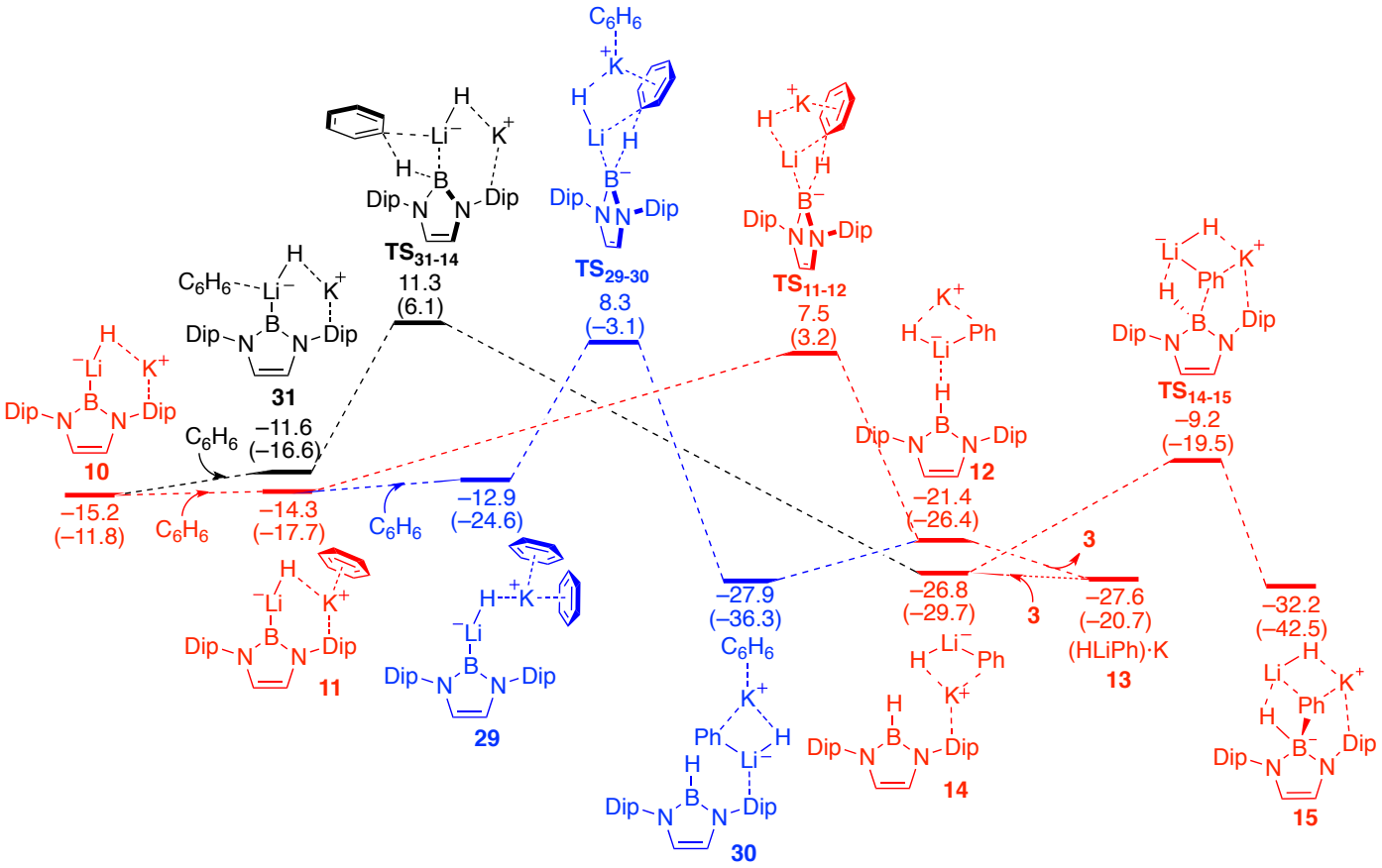

Scheme S4. Energy profiles calculated for deprotonation of the second benzene by **10**. The relative Gibbs free energies and electronic energies (in parentheses) are given in kcal/mol.

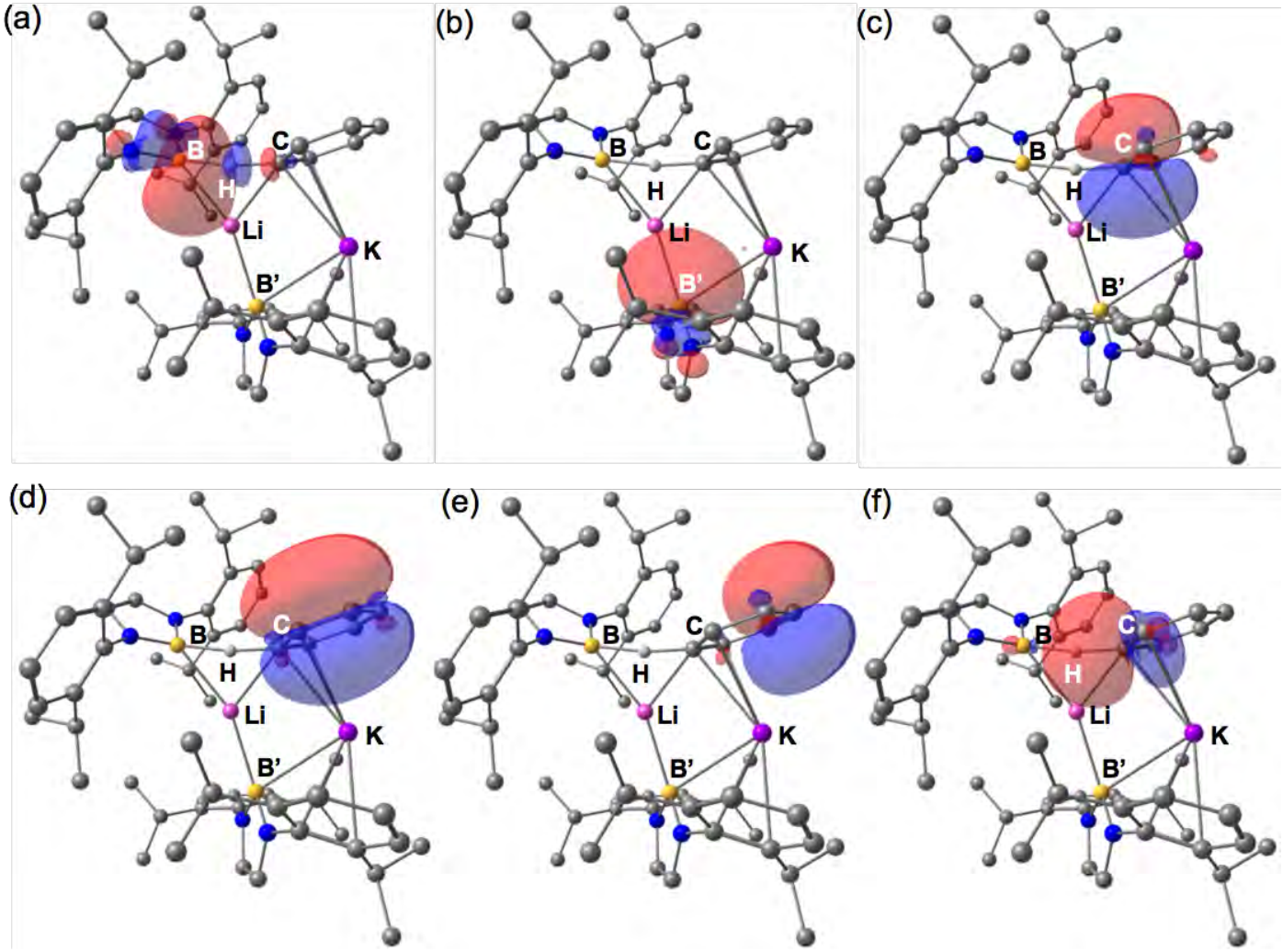

Figure S10. Natural orbitals (a) 243, (b) 242, (c) 228, (d) 225, (e) 223, and (f) 220 on the optimized transition state $\mathbf{TS_{2\text{-}6}}$ for the deprotonation of benzene by **2**, showing donor-acceptor interactions (isovalue = 0.02); hydrogen atoms except for those being deprotonated are omitted for clarity; white: hydrogen, gray: carbon, blue: nitrogen, yellow: boron, deep purple: potassium, light purple: lithium)

References for Supporting Information

[1] Y. Segawa, Y. Suzuki, M. Yamashita, K. Nozaki, *J. Am. Chem. Soc.* **2008**, *130*, 16069-16079.

[2] Y. Segawa, M. Yamashita, K. Nozaki, *Science* **2006**, *314*, 113-115.

[3] (a) C. Kabuto, S. Akine, T. Nemoto, E. Kwon, *J. Cryst. Soc. Jpn.* **2009**, *51*, 218-224; (b) C. Kabuto, S. Akine, E. Kwon, *J. Cryst. Soc. Jpn.* **2009**, *51*, 218-224.

[4] M. C. Burla, R. Caliandro, B. Carrozzini, G. L. Cascarano, C. Cuocci, C. Giacovazzo, M. Mallamo, A. Mazzone, G. Polidori, *J. Appl. Crystallogr.* **2015**, *48*, 306-309.

[5] G. Sheldrick, *Act. Cryst. Sec. C* **2015**, *71*, 3-8.

[6] (a) C. Lee, W. Yang, R. G. Parr, *Phys. Rev. B* **1988**, *37*, 785-789; (b) A. D. Becke, *Phys. Rev. A* **1988**, *38*, 3098-3100; (c) B. Miehlich, A. Savin, H. Stoll, H. Preuss, *Chem. Phys. Lett.* **1989**, *157*, 200-206; (d) A. D. Becke, *J. Chem. Phys.* **1993**, *98*, 5648-5652; (e) P. J. Stephens, F. J. Devlin, C. F. Chabalowski, M. J. Frisch, *J. Phys. Chem.* **1994**, *98*, 11623-11627.

[7] S. Huzinaga, J. Andzelm, M. R.-A. Klobukowski, Esakai, Y., H. Tatewaki, *Gaussian basis sets for molecular calculations*, Elsevier, **1984**.

[8] M. J. Frisch, G. W. Trucks, H. B. Schlegel, G. E. Scuseria, M. A. Robb, J. R. Cheeseman, G. Scalmani, V. Barone, B. Mennucci, G. A. Petersson, H. Nakatsuji, M. Caricato, X. Li, H. P. Hratchian, A. F. Izmaylov, J. Bloino, G. Zheng, J. L. Sonnenberg, M. Hada, M. Ehara, K. Toyota, R. Fukuda, J. Hasegawa, M. Ishida, T. Nakajima, Y. Honda, O. Kitao, H. Nakai, T. Vreven, J. A. Montgomery Jr, J. E. Peralta, F. Ogliaro, M. J. Bearpark, J. Heyd, E. N. Brothers, K. N. Kudin, V. N. Staroverov, R. Kobayashi, J. Normand, K. Raghavachari, A. P. Rendell, J. C. Burant, S. S. Iyengar, J. Tomasi, M. Cossi, N. Rega, N. J. Millam, M. Klene, J. E. Knox, J. B. Cross, V. Bakken, C. Adamo, J. Jaramillo, R. Gomperts, R. E. Stratmann, O. Yazyev, A. J. Austin, R. Cammi, C. Pomelli, J. W. Ochterski, R. L. Martin, K. Morokuma, V. G. Zakrzewski, G. A. Voth, P. Salvador, J. J. Dannenberg, S. Dapprich, A. D. Daniels, Ö. Farkas, J. B. Foresman, J. V. Ortiz, J. Cioslowski, D. J. Fox, Gaussian, Inc., Wallingford, CT, USA, **2013**.

[9] A. E. Reed, L. A. Curtiss, F. Weinhold, *Chem. Rev.* **1988**, *88*, 899-926.

[10] (a) F. London, *J. Phys. Radium* **1937**, *8*, 397-409; (b) R. Mcweeny, *Phys. Rev.* **1962**, *126*, 1028-1034; (c) R. Ditchfield, *Mol. Phys.* **1974**, *27*, 789-807; (d) K. Wolinski, J. F. Hinton, P. Pulay, *J. Am. Chem. Soc.* **1990**, *112*, 8251-8260; (e) J. R. Cheeseman, G. W. Trucks, T. A. Keith, M. J. Frisch, *J. Chem. Phys.* **1996**, *104*, 5497-5509.

[11] T. A. Keith, (version 14.04.17) ed., TK Gristmill Software, Overland Park KS, USA, **2014**.

[12] S. W. Benson, *The Foundations of Chemical Kinetics*, Krieger, Malabar, FL, **1982**.

[13] S. Grimme, S. Ehrlich, L. Goerigk, *J. Comput. Chem.* **2011**, *32*, 1456-1465.

[14] (a) M. Cossi, V. Barone, R. Cammi, J. Tomasi, *Chem. Phys. Lett.* **1996**, *255*, 327-335; (b) M. Cossi, V. Barone, B. Mennucci, J. Tomasi, *Chem. Phys. Lett.* **1998**, *286*, 253-260; (c) M. Cossi, V. Barone, M. A. Robb, *J. Chem. Phys.* **1999**, *111*, 5295-5302; (d) M. Cossi, N. Rega, G. Scalmani, V. Barone, *J. Comput. Chem.* **2003**, *24*, 669-681.